Coupling light to periodic nanostructures

Driessen, E.F.C.

Chapter 4

Imaging of a Fano resonance in a two-dimensional photonic-crystal slab

We investigate a resonance of a photonic-crystal slab by imaging the reflection from the slab of a strongly focused beam of monochromatic light. Polarization-dependent k-space imaging allows us to identify the resonance as originating from diffraction into a TM_0 waveguide mode. In real-space images of the reflection, we can spatially separate the direct and resonant contributions of the Fano resonances that are observed in the reflection spectra. We observe decay lengths of the resonant contributions of up to 7 μm. From the normal-incidence reflection spectrum we determine the escape rate. Combined, this allows us to estimate a group refractive index $n_g = 2.6$ and a phase index $n_{eff} = 1.5$ of the resonant mode.

4.1 Introduction

Reflection spectra from waveguides that are patterned with a periodic array of holes, so-called photonic-crystal slabs, contain a multitude of sharp, resonant features. These features are caused by diffraction from the periodic array of holes into a (leaky) waveguide mode. Light that is coupled into these leaky modes diffracts back, and interferes with the direct (Fresnel) reflection from the layered structure. This interference leads to the typical asymmetric (Fano) line shape as described in the previous chapters. Usually, information about the dispersion of these resonances is only obtained by measuring spectra at different angles of incidence [20]. These spectra are compared to calculations, and information about the resonance is distilled, most notably the specific waveguide mode that the light is coupled into. This method has the obvious disadvantage that it only works well for structures of which the constitution is reasonably well known, but even then, complications arise, since TE waveguide modes can show up in *p*-polarized reflection spectra, and vice-versa [46].

In this chapter, we use a different approach to obtaining information about a specific resonance of a photonic-crystal slab. We use a strongly focused, monochromatic beam to illuminate the photonic crystal at a specific spot. We image the reflection of the sample both in real space and in k-space. From the k-space images, we were able to unambiguously identify the resonance as a first-order diffraction process into the TM_0 waveguide mode. Real-space images allow us to separate the resonant and non-resonant contributions of the Fano resonance. In these images, we can measure the decay length of the resonant contribution directly. From this length and the decay time, obtained from a separate measurement of the reflection spectrum, we can determine the group refractive index of the leaky waveguide mode.

4.2 Sample

The photonic-crystal slab used in this chapter is made using the techniques described in Ch. 2. It consists of a 160 nm thick, free-standing membrane of $Al_{0.35}Ga_{0.65}As$ that is patterned with a 250×250 μm^2 large square array of holes with a radius $r \approx 120$ nm and a lattice constant $a = 480$ nm. Due to a small lattice mismatch of the lattice constants of the AlGaAs and the GaAs substrate, there is a small compressive strain in the membrane layer, that is released when the sacrificial layer is etched. This causes the membrane layer to buckle up, resulting in a variable distance between the membrane and the GaAs substrate when moving along the membrane.

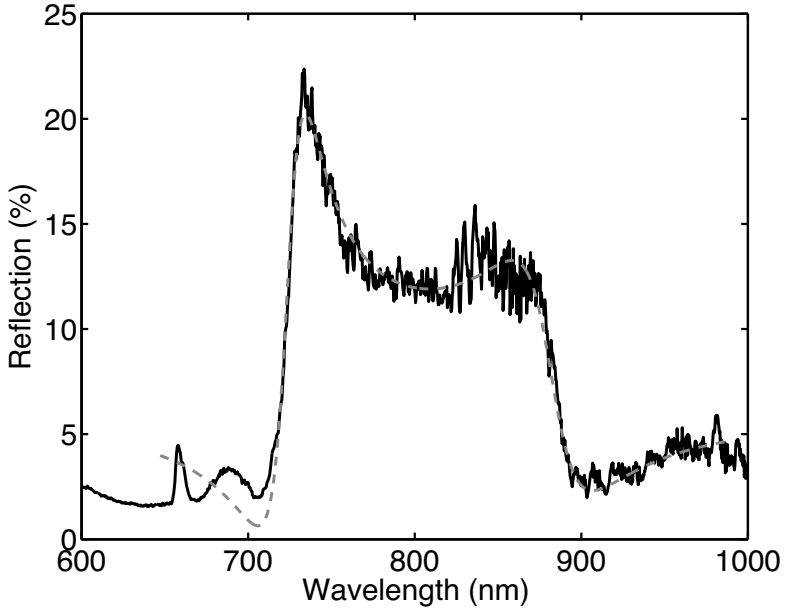

Figure 4.1. Normal-incidence reflection spectrum of the photonic-crystal membrane (solid curve). Two asymmetric Fano resonances are visible, centered around wavelengths of 725 nm and 882 nm. The dashed curve is a fit of a Fano model with two resonances to the measurements, as discussed in the text.

4.3 Normal-incidence reflection spectrum

The photonic-crystal slab two distinct resonances in the near-infrared spectral region. Figure 4.1 shows the reflectivity of the membrane at normal incidence, as a function of the wavelength of the incident light. To record this curve, we used an unpolarized, fiber-coupled xenon lamp and imaged the 50 μm-diameter fiber facet onto the sample, while limiting the numerical aperture of the incident light to < 0.01. The reflected light was collected with a 200 μm core-size fiber and sent to a grating spectrometer*, to analyze the spectral content. The detected signal was normalized to the reflection from a silver mirror.

The measurement in Fig. 4.1 shows two asymmetric (Fano) resonances, centered around wavelengths of 725 nm and 882 nm. We ascribe the small peak that is observed around 670 nm to luminescence at the band edge of

*Ocean Optics USB2000, resolution 1.2 nm.

the AlGaAs material, and not to a resonance that is caused by the patterning of the membrane. This assumption is confirmed by the fact that the peak does not change spectral position when changing the angle of incidence of the illumination. To obtain a better understanding of the reflection spectrum, we used the Fano model described in Ch. 2. In this model, the reflection is given by

$$R = \left| r - \sum_p \gamma_p \frac{r \pm it}{i(\omega - \omega_p) + \gamma_p + \Gamma_p} \right|^2 , \tag{4.1}$$

where r and t are the reflection and transmission coefficients of the direct contribution, respectively, ω is the angular frequency of the light, ω_p the resonance angular frequency, γ_p the radiative loss, and Γ_p the irreversible (scattering) loss of waveguide mode p. In order to fit this model to the measurements, we assumed that the reflection r is constant over the wavelength range. Furthermore, we assumed that the transmission t is given by $|t|^2 = 1 - |r|^2$, i.e. that there are no losses in the direct channel. We checked this assumption by adding some loss in the direct channel (i.e., $|r|^2 + |t|^2 < 1$). This addition of loss did not change the overall quality factor $Q = \omega_p/(\gamma_p + \Gamma_p)$ of the resonances significantly. It does change the relative contributions of γ_p and Γ_p in Eq. (4.1), which makes a reliable independent fit of these two parameters impossible. The buckling of the membrane structure causes a variable distance between the free-standing membrane and the GaAs substrate. This results in an ambiguity of both the precise angle of incidence and the vertical structure of the different layers. Combined, this makes it impossible to calculate the Fresnel coefficients for direct reflection and transmission for this structure, contrary to the structure discussed in chapters 2 and 3.

The dashed curve in Fig. 4.1 shows the best fit of this model to the measurements. The fit parameters are summarized in Table 4.1. The fit was performed using two resonances with opposite symmetry [set by the $\pm$ sign in Eq. (4.1)]. The symmetry of the two resonances in Fig. 4.1 is determined by the symmetry (even or odd) of the waveguide modes relative to the plane in the middle of the slab [30]. For the wavelength range of these measurements, the only two waveguide modes that are below cut-off are the TM_0 and the TE_0 waveguide mode. Since these two waveguide modes have opposite symmetry, we conclude that each of the two resonances is caused by coupling to a different waveguide mode. Since the phase of the direct reflection cannot be determined from this measurement, it is impossible to tell from the shape of the resonant peaks, which resonance corresponds to which specific waveguide mode, however.

Table 4.1. Fit parameters and 95% confidence intervals of the two-resonance Fano model.

Parameter	Value	
	Resonance 1	**Resonance 2**
r	0.238 ± 0.002	
$2\pi c/\omega_p$ (nm)	725.4 ± 0.3	881.8 ± 0.6
Q	53 ± 1	37 ± 1

4.4 Imaging of the resonance

In order to gain more insight into the character of the resonance around 725 nm, we image the reflection of a strongly focused beam of light from the photonic crystal slab. Figure 4.2 shows a schematic overview of the setup used in the experiments. Light from a tunable picosecond Ti:Sapphire laser or from an external-cavity tunable diode laser is attenuated using neutral-density filters (ND), sent through a single-mode optical fiber (SMF), and collimated with a $f = 5$ cm lens to a beam of ~ 1 cm diameter. The beam is polarization-filtered using a polarizer (P). A glass plate that is anti-reflection coated on one side is used as a beam splitter (BS) to direct the beam to an aspheric lens L3 ($f = 8$ mm, NA $= 0.5$), that focuses the light onto the photonic-crystal membrane. The membrane is aligned such that the beam axis is parallel to its surface normal. The reflection from the membrane is collected with the same lens and sent back onto the beam splitter. The reflected light is transmitted through this beam splitter, and the surface of the photonic crystal membrane is imaged onto a CCD camera using a $f = 250$ mm lens L4. A second lens L5 ($f = 125$ mm) can be inserted into the imaging setup, to make a k-space image of the photonic crystal reflection. The solid and hatched beam paths depicted in Fig. 4.2 show the imaging of the real-space and k-space reflection, respectively. A polarization analyzer was placed between lenses L4 and L5 to probe the polarization properties of the reflected light.

For our experiments, we selected a part of the membrane that was locally parallel to the GaAs substrate, to minimize the pattern of interference fringes caused by the (partial) reflection from the substrate of light that was transmitted through the membrane. We recorded the real-space and k-space reflection image of an unpatterned piece of the substrate next to the membrane, as a reference. We aligned the crystal axes of the photonic crystal such, that the ΓX-directions were parallel to the horizontal and vertical directions of the images.

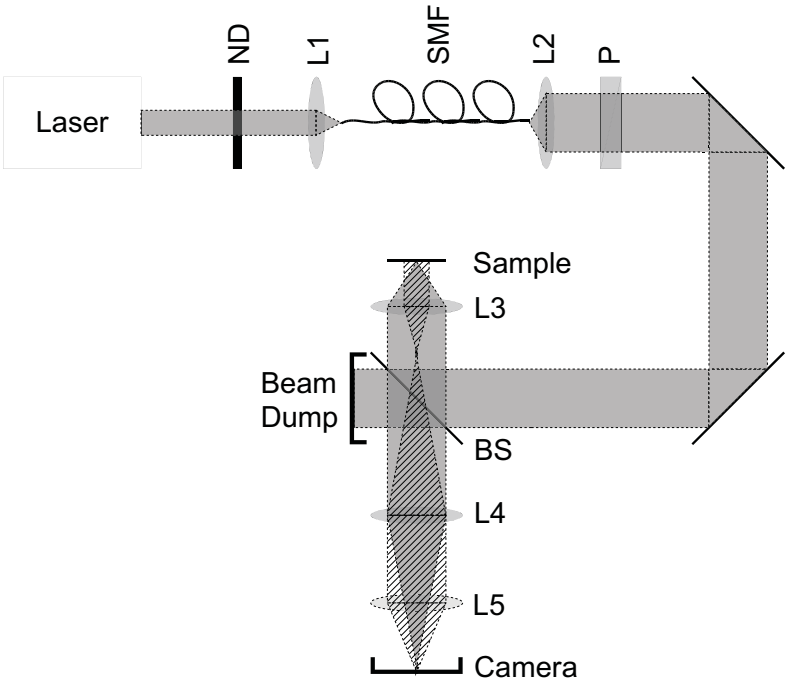

Figure 4.2. Experimental setup. Light from a tunable laser is focused on the photonic-crystal sample via a beam splitter (BS). By inserting the lens L5, the imaging is switched from real-space imaging (solid beam path) to k-space imaging of the reflection from the photonic crystal slab (hatched beam path). Details of the setup are found in the text.

4.4.1 k-space imaging and polarization properties

Figure 4.3(a) shows the recorded reflection in k-space, when the photonic-crystal slab was illuminated at a wavelength of 762.5 nm, red-detuned from the resonance at 725 nm, with horizontal polarization. Most obviously, a dark and bright ring pattern, that is centered around the normal-incidence (Γ) point (the center of the image) is visible. These Fabry-Perot fringes are caused by the partial reflection from the GaAs substrate underneath the photonic-crystal slab, that interferes with the reflection from the slab. The fact that the rings are concentric indicates that locally the membrane is parallel to the GaAs substrate.

Besides the Fabry-Perot fringes, a resonance is observed on the left and right sides of the normal-incidence point. Most obviously, the dark minimum of the Fano resonance is observed. The azimuthal angular dependence of the

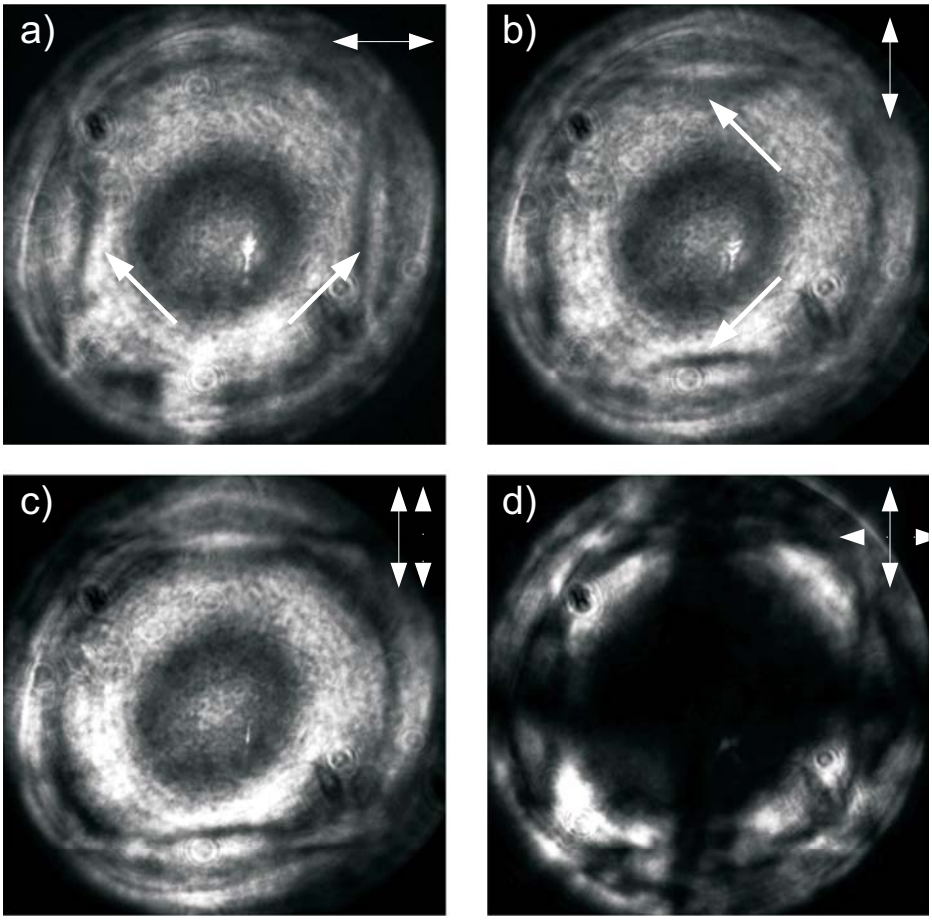

Figure 4.3. k-space image of the reflection of the photonic-crystal slab, when illuminated at a wavelength of 762.5 nm. (a) and (b) show the reflection when no analyzer is placed in the detection path and the illuminating light was polarized horizontally (a) and vertically (b). In these images, a resonance is visible (indicated with the arrows). In figures (c) and (d), the illumination was polarized vertically, and an analyzer was placed in the detection path, either parallel (c) or perpendicular (d) to the polarizer. The full image spans a numerical aperture $NA = 0.5$. The solid arrows in the upper right corner of the figures indicates the polarizer setting, the dashed arrows indicate the analyzer settings.

resonance suggests that the resonance originates from the $(\pm 1, 0)$ reciprocal lattice points. The resonances are not visible in the vertical direction. When the polarization of the illumination is rotated 90° (b), only the resonances in the $(0, \pm 1)$ direction are visible. A comparison with a calculation of the waveguide modes of a uniform slab with an effective refractive index (not shown), and folding these modes back into the first Brillouin zone, confirms that the resonance is caused by coupling to the TM_0 waveguide mode, by diffraction from the (1,0) reciprocal lattice points. On changing the wavelength towards the blue, the resonances are observed to shift towards the Γ-point. This allows us to identify this resonance with the resonance around 725 nm, observed in the normal-incidence reflection spectrum.

Figures 4.3(c) and (d) show a polarization analysis of the reflection for vertically polarized light. In Fig. 4.3(c), an analyzer is placed parallel to the polarization of the incident light. In Fig. 4.3(d), the analyzer is placed perpendicularly. Most of the reflected light is polarized the same as the incident light, except for four small areas in the (diagonal) ΓM-directions. Along the directions of high symmetry, the resonances of a photonic-crystal slab can be characterized by the polarization properties of the radiating field, as either *s*- or *p*-polarized [38]. The incident polarization is aligned with the ΓX symmetry direction, such that it is *p*-polarized in the vertical, and *s*-polarized in the horizontal direction. Since these are the eigenpolarizations of the resonant modes, no polarization mixing occurs and the reflected light has the same polarization as the incident light. Away from the ΓX directions, the incident light is both *s*- and *p*-polarized, nor polarized in an eigenpolarization of the resonant mode. Light that is coupled into the leaky waveguide mode will therefore undergo a polarization rotation, which shows up in the *k*-space image with crossed polarizers [Fig. 4.3(d)].

4.4.2 Real space imaging

Figure 4.4 shows the real-space reflection of the photonic-crystal slab, using the same illumination conditions as before, for horizontally (a) and vertically (b) polarized illumination, on a logarithmic scale. Besides a very bright spot where the slab is illuminated, two tails are visible, in the direction of the incident polarization. These tails are formed by light that is coupled into a leaky waveguide mode, and propagates in this mode before being diffracted back. The fact that we only observe a tail parallel to the incident polarization confirms again that the mode we couple into is a TM-like waveguide mode. The distortions in the images are caused both by the fact that the membrane is not flat, and could also be due to the fact that a resonantly excited mode propa-

gates in the direction of the group velocity, which is not necessarily the same as the direction of the reciprocal lattice vector that causes the resonance [47, 48].

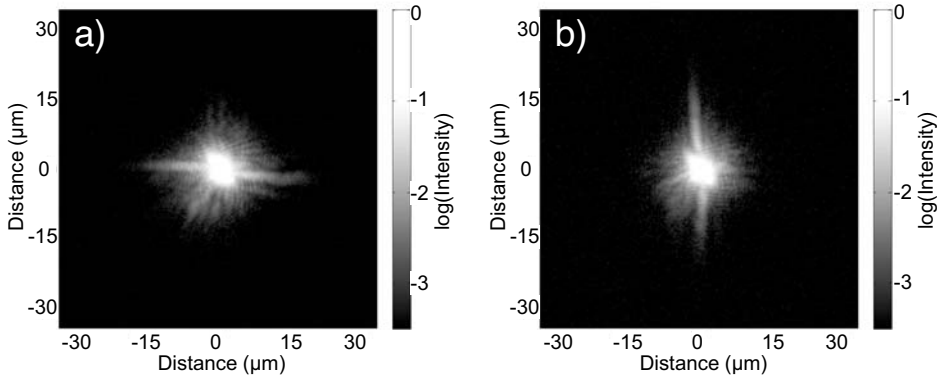

Figure 4.4. Real space image of the reflection of the photonic-crystal slab, when illuminated at a wavelength of 762.5 nm, on a logarithmic scale, for horizontally (a) and vertically (b) polarized illumination. The two long tails that emerge from the pump spot are caused by light that is resonantly coupled to a leaky waveguide mode of the slab, and that decays exponentially from this waveguide mode.

In Fig. 4.5 we show a cross-section of the vertical resonance of Fig. 4.4(b). To obtain this plot, we summed the intensity over a horizontal box of width 4.5 μm, in order to capture all intensity in the resonant tails. In this image, the direct and resonant contributions to the Fano resonance are spatially separated [49]. The central peak is Gaussian in shape, and corresponds to a direct image of the illuminating spot. As a comparison, the reflection from an unpatterned piece of the sample is given as the dash-dotted curve, showing a perfect agreement with the peak of the measured curve. The resonant tails decay exponentially on both sides of the central spot. A fit of a single exponential to these tails is shown by the dashed lines. The resonant contribution can be traced over 2.5 orders of magnitude, and up to a distance of 30 μm away from the center of the illumination spot. An interference between the resonant and non-resonant contributions, as observed in similar experiments with surface-plasmon polaritons [49], was not observed in these measurements.

We measured the real-space image of the resonance for different wavelengths from 700 to 800 nm. From these images, we obtained the decay length of the resonant contribution by fitting a single exponential to the intensity of the resonant tail. The result of these fits are shown in Fig. 4.6 and varies from ~ 3 μm at wavelengths around 750 nm to ~ 7 μm at 795 nm.

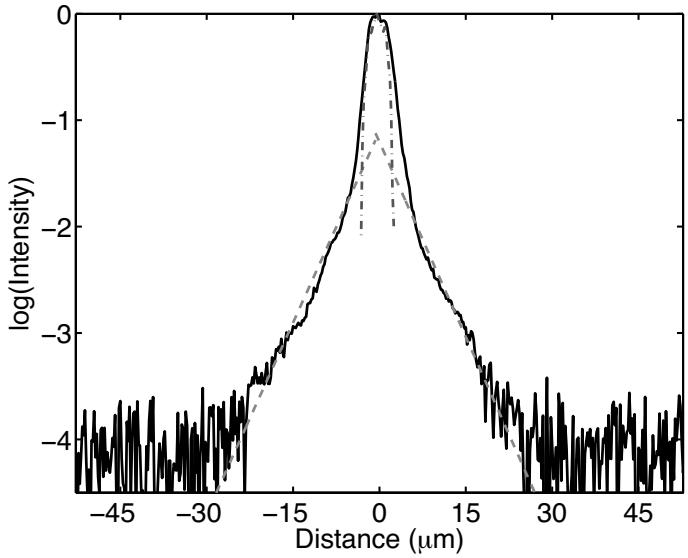

Figure 4.5. Logarithmic plot of the measured reflected intensity, taken along the vertical resonance in Fig. 4.4(b) (solid curve). The two contributions to the Fano resonance are spatially separated. The reflection arising from the direct (Fresnel) contribution is giving rise to the central spot, whereas the exponentially decaying tails are caused by light that is resonantly coupled to a waveguide mode. The dashed lines show a linear fit to the resonant tails. The dash-dotted curve is the profile of the pump spot, measured on an unpatterned region of the substrate.

The decay length l of the resonant tails can be parametrized by

$$l = \frac{v_\mathrm{g}}{\gamma + \Gamma} = \frac{\lambda}{2\pi n_\mathrm{g}} Q, \tag{4.2}$$

where v_g and n_g are the group velocity and the group index, respectively, γ and Γ are the escape rates as defined before, and λ is the wavelength of the light in vacuo. Q is the quality factor of the resonance, as defined before. Using this equation, we determine the group refractive index at normal incidence (725 nm) to be 2.6. Although this value is small compared to the refractive index of the AlGaAs material ($n \approx 3.5$), it is large compared to the effective index of the TM_0 waveguide mode of the slab, which we estimate to be $n_\mathrm{eff} \approx 1.5$. This estimate was made noting that the resonance at the Γ point occurs when the condition $\lambda = n_\mathrm{eff} a$ is met, and assuming no avoided crossing around the Γ-point. At this wavelength, the TM_0 waveguide mode is still very close to cut-off, which explains why the calculated effective index of the waveguide mode

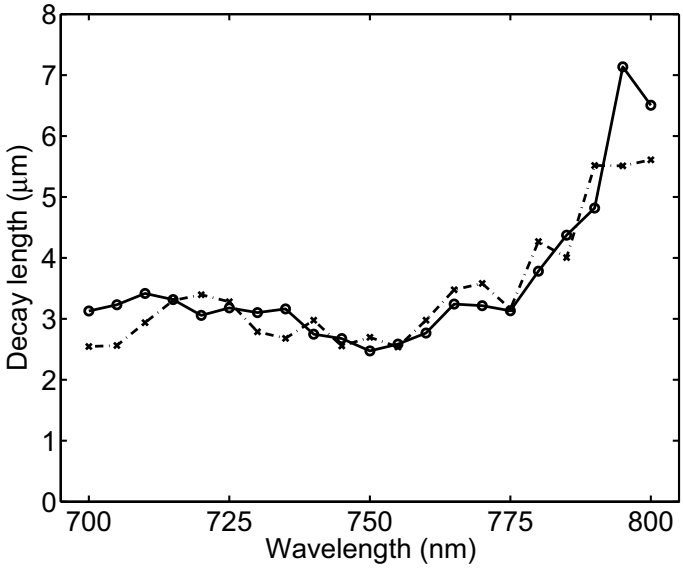

Figure 4.6. Decay length of the $TM_0(1,0)$ resonance as a function of wavelength. The circles and crosses show the fitted decay length on either side of the non-resonant reflection spot. The lines are guides to the eye.

is so close to the refractive index of the surrounding air. The group index is actually comparable to both the group index calculated from the waveguide dispersion of an unpatterned waveguide, and to the group index that is caused by the refractive-index dispersion of the AlGaAs material. We do not observe a considerable increase of the group index around the band gap at the Γ point. This is due to our illumination scheme where we illuminate the photonic crystal with a high numerical aperture. We therefore excite the resonance at different angles of incidence, but the resonance that is excited with the largest decay length, i.e. the highest group velocity, will be most pronounced in the imaging.

The variation of the decay length with wavelength can be explained as follows: both the group index and the decay time of the resonance change with changing angle of incidence. The group index is proportional to $(\partial\omega/\partial k)^{-1}$. At the Γ-point, an avoided crossing occurs. The resonant modes consist of standing waves, which causes $n_g \rightarrow \infty$. When moving the resonance away from the Γ point, the group index will lower, leading to a longer decay length. At the same time, the decay time will change [38], which also leads to a change in decay length, as observed in the measurements. Some precaution has to be taken with the resonance that is observed at 883 nm. With increasing angle

of incidence, we expect this resonance to split, and obtain a branch that shifts to lower wavelengths. Since this resonance can be linked to a TE waveguide mode, however, we do not expect this resonance to couple strongly to the TM-like resonance that is described in the rest of this chapter.

4.5 Conclusion

The imaging technique described in this chapter allowed us to directly measure the decay length of a photonic-crystal resonance. In principle, this decay length can be linked to the group refractive index at this specific wavelength. This would require exact knowledge of the variation of the resonance decay time with wavelength, which could be obtained by measuring the reflection spectra of the photonic-crystal slab at different angles of incidence, which in turn would also yield the group refractive index. The advantage of the technique used in this chapter lies in the fact that an unambiguous identification of the specific waveguide mode and reciprocal lattice vector is possible using a k-space image. Moreover, it allows to spatially separate the resonant and non-resonant contributions of a Fano resonance, which is principally impossible using a series of reflection spectra.